

Imaging near-surface defects using step-frequency ground-penetrating radar

V.R. Balasubramaniam^{1*}, P.C. Jha¹ and E. Chandrasekhar²

¹ National Institute of Rock Mechanics, Champion Reefs, P.O., Kolar Gold Fields-563117, India

² Department of Earth Sciences, Indian Institute of Technology Bombay, Powai, Mumbai-76, India

Received October 2011, revision accepted September 2012

ABSTRACT

Step-Frequency GPR (SFGPR) investigations were carried out at the location of a crude oil storage tank at a petroleum refinery. The storage tank was founded on an elevated platform (tank-pad). Subsidence of a portion of the tank-pad led to cracking of its bottom steel plates and subsequent leakage of crude oil. SFGPR imaging was done within and outside the tank, in the frequency range of 10–260 MHz, to understand the cause of the subsidence. Complex signal analysis was useful in identifying a series of cavities in the subsurface, in the depth range of 2–15 m, close to the location of subsidence of the tank-pad. In order to stabilize the foundation of the tank, the subsurface area infested with cavities was grouted systematically. SFGPR imaging was done again after grouting, in the same area in the same manner to evaluate the efficacy of grouting and check for presence of remnant cavities. Results of the SFGPR investigations, before and after grouting, which aided restoration of the foundation of the oil tank, are discussed.

INTRODUCTION

Construction of large structures is normally done on a strong foundation so that it is sustainable during its lifespan. Despite cognizance of the subsurface conditions based on routine investigations before construction, it is sometimes possible that some hidden features in the foundation like loose-soil pockets (unconsolidated) or cavities in the subsurface escape attention. Such subsurface defects, if present in the foundation, prove detrimental to the stability and longevity of a structure due to uneven settlement of the ground. In the unexpected event of damage to a superficial structure, scientific investigations to find an engineering solution become imperative. Geophysical investigations can be a useful aid in such engineering solutions.

Various geophysical techniques have been employed for mapping near-surface features such as cavities or voids and sinkholes. The seismic reflection technique (Cook 1965; Miller and Steeples 1991), electrical and electromagnetic methods (Labuda and Baxter 2001; Pellerin 2002; Cardarelli *et al.* 2006), microgravity (Butler 1984; Branston and Styles 2006) and magnetic methods (Rybakov *et al.* 2005) have all yielded satisfactory results. There have also been successful applications of integrated geophysical techniques for mapping near-surface features (Beres *et al.* 2001; Mochales *et al.* 2008; Bavusi *et al.* 2009). Integrated techniques are aptly suited to map such subsurface features because each technique gives specific information about the feature with the respective physical parameter associated to it.

Among various geophysical techniques, ground-penetrating radar (GPR) has been recognized as a reliable technique for imaging near-surface features. GPR uses the transmission and reception of high-frequency (10–3000 MHz) electromagnetic (EM) waves for imaging near-surface features. Propagation of the high-frequency EM waves in the subsurface is governed by the electrical properties (Olhoeft 1998) of the medium. More information on the principle and modulation techniques of GPR can be found in the works of Daniels (1996) and Davis and Annan (1989). With significant advancements in the field of electrical and electronics technology, GPR has evolved as a more portable high-resolution non-destructive imaging tool with wide ranging applications. Quick deployment and real time visualization and analysis of signals have given the GPR an advantage of imaging in relatively lesser time and cost compared to other geophysical techniques. The efficacy and reliability of GPR in detecting near-surface cavities or voids, caves and tunnels (Ballard *et al.* 1983; Daniels 1988; Benson 1995; Chamberlain *et al.* 2000; Xu *et al.* 2010) has been proven. In all these works, one of the variants of GPR, Impulse Ground-Penetrating Radar (IGPR) was used, which is a first generation GPR that uses a short impulse (0.6–10 ns) and operates in the time domain.

Another variant of GPR called Step-Frequency GPR (SFGPR) is a second generation GPR, which uses a synthetic pulse and operates in the frequency domain. SFGPR has advantages (Robinson *et al.* 1974) over conventional IGPR like the capability to detect a target in high-loss media (Lizuka *et al.* 1984), controlled transmission of coherent signals and efficient

* vrbala.nirm@gmail.com

use of high-transmitter and receiver powers (Noon *et al.* 1994), ability to modify the signal bandwidth (Kong and By 1995), enhanced dynamic range (Hamran *et al.* 1995), improved penetration depths (Stickley *et al.* 2000) and sophisticated spectral control (Langman and Inggs 2001). Though SFGPR has been shown to have theoretical advantages, there are some practical disadvantages like complicated hardware, cable radiation, lower bandwidth, strong direct coupling and longer recording time as reported by Leckebusch (2011), Kong and By (1995) and Stickley *et al.* (2000). Taking cognizance of the merits and disadvantages, we made an attempt to apply SFGPR for imaging near-surface cavities, voids or subsurface defects below large structures.

In the present study, conducted at a petroleum refinery, the SFGPR (By *et al.* 1992; Kong and By 1995) developed at the Norwegian Geotechnical Institute (NGI), was used. The results of the investigations are analysed, in imaging the defects in the foundation of an oil storage tank and in assessing the efficacy of grouting in annulling these defects.

STEP-FREQUENCY GROUND-PENETRATING RADAR

The step-frequency (SF) version is a second generation GPR, which uses continuous waveform and whose frequency is stepped up over a number of narrow bands sequentially (Kong and By 1995; Hamran *et al.* 1995). The operating principle and the performance of this radar, which uses a signal generator and receiver unit, were described in detail by Kong and By (1995).

Mathematically, a continuous sinusoidal step-frequency signal is represented as (Kong and By 1995)

$$f(t) = A \exp(i2\pi(f + n\Delta f)t) \quad \frac{n-1}{N}T \leq t \leq \frac{n}{N}T$$

where A is the amplitude of the signal and $n\Delta f$ designates the n^{th} frequency step interval Δf , N is the total number of step frequencies and T is the fundamental period of the signal. The SFGPR transmits waveform frequency tones stepped with Δf , which are highly stable and uniformly spaced across a wide fractional bandwidth.

The step-frequency technique is one of the many hardware options for transmitting signals with wide fractional bandwidths and high mean power. It has the capability of using the desired bandwidth of the transmission signal within a resonant frequency bandwidth for a given ground condition, thereby optimizing the antenna performance in tune with the objective of the imaging. SFGPR is characterized by a wide dynamic range and is capable of imaging deeper targets with a lesser power requirement. Since this radar uses the source signal in the frequency domain, ambiguity in the bandwidth of the received signal spectrum is less.

SFGPR equipment comprises five units, *viz.* network analyser (NA), which is the radar signal transmitter-receiver unit, radio frequency (RF) amplifiers, a portable computer (PC), a pair of RF coaxial cables and a pair of transmitter (Tx) and receiver antennae (Rx) (Jha *et al.* 2006). The NA used in this SFGPR is

capable of transmission and reception of radio waves in the frequency range of 0.3–3000 MHz over a dynamic range of 110 dB. It transmits and receives the radar signal in sequential steps of 51, 101 and 201, as optionally chosen during data acquisition. External RF amplifiers are used to amplify the radar signals during transmission and reception whereby the dynamic range of the system is further enhanced. The portable computer, using tailor-made software with built-in modules for the selection of survey parameters, data acquisition, display and preprocessing of the received signals, is used to control operations of SFGPR during the survey through a PCMCIA-GPIB (National Instruments) interface. The antennas are designed for a particular centre frequency to perform the ultra-wideband operation. The Tx and Rx are an identical pair of antennas measuring 2 m in length and 0.2 m in width and are flat conductor dipole antennas with a centre frequency of 50 MHz. They are ground coupled antennas, designed to feed power into the ground efficiently (Kong and By 1995). They are connected to the NA through RF cables. Suitable bandwidth for scanning is selected based on the response of the ground. Low-porosity manganese-zinc (Mn-Zn) ceramic ferrites cores are mounted on these RF cables to suppress RF leakage and cross-coupling during data acquisition. The apparent disadvantages of this version of SFGPR are its bulky NA and the long cables. However, the distinguishable advantages of this GPR *viz.* frequency synthesized (stepped) signals, improved sensitivity and the software based ability to modify the bandwidth of the signals to optimize antenna performance as per the site conditions, make this a useful tool for detection of shallow and deep targets (Kong and By 1995).

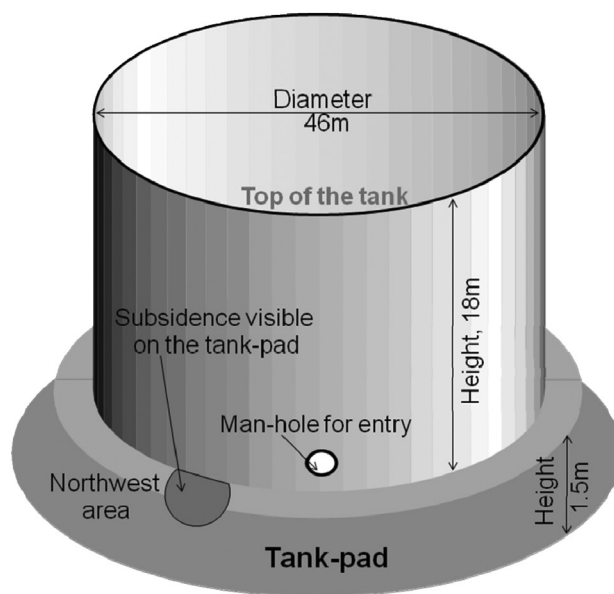


FIGURE 1
Perspective view of the oil storage tank shown with the location of subsidence (dark-shade semi-circle).

DEFINITION OF THE PROBLEM

The petroleum refinery had a number of oil tanks commissioned for the purpose of storing crude oil products at different stages of processing. The oil storage tanks were normally self-sustaining superficial structures erected on an elevated platform (tank-pad), which were made of a well-consolidated mixture of stone chips and sand covered by bitumen. The near-surface stratum in the refinery area was predominantly characterized by lateritic soil in various degrees of hardness and compaction with a small percentage of coastal alluvium. One of the oil tanks measuring 46 m in diameter and 18 m in height was made up of 16 mm thick steel plates. The tank was installed on a 1.5 m thick tank-pad. A perspective view of the tank and the visible subsidence area in the tank-pad are shown in Fig.1. The tank-pad was subjected to standard load tests to check for settlement of the ground. Once the tank-pad passed all the tests, the tank was commissioned into the production process. However, within one year of its commissioning, the bottom steel plates of the tank cracked and resulted in leakage of all the stored crude oil. Subsidence in the tank-pad was observed close to the damaged portion of the bottom plates of the oil tank. Such a failure was unique in the history of the refinery as there were several such tanks installed on a similar foundation, which withstood operational success for more than ten years (Jha *et al.* 1999). Initially, failure of the material used for welding of the bottom plates was suspected as the cause. However, examination of the bottom plates and the weld material proved their worthiness for use in such tanks. At this stage, presence of some unknown defect in the subsurface was suspected, due to which the tank bottom plates might have cracked. Previously, tunnel-like features were observed in the subsurface at a nearby site where excavations were in progress. Thus, non-destructive geophysical investigation at the site using SFGPR was employed to investigate the subsurface in and around the area of subsidence in the tank-pad, with the goal of understanding the cause of the subsidence.

DATA ACQUISITION

SFGPR data were acquired along a series of orthogonal lines in a grid pattern both inside and outside the oil tank around the visible subsidence in the tank-pad. Inside the tank, measurements were made on the tank-pad after removing the bottom plates. Figure 2 depicts the schematic plan view of the SFGPR survey lines. The dense grid lines with 2 m x 2 m spacing were chosen to have wider data coverage for better understanding of the extent and orientation of the suspected subsurface defects. The SFGPR survey was done in common offset mode using antennas of 50 MHz centre frequency oriented transverse to the line of survey with a separation of 2 m and a movement step of 0.5 m in the frequency range of 10–260 MHz transmitted over 201 steps. In order to estimate the velocity of the radio waves in the subsurface, a common midpoint (CMP) survey was carried out at two locations, one inside and one outside the tank. SFGPR data acquisition was done before grouting for under-

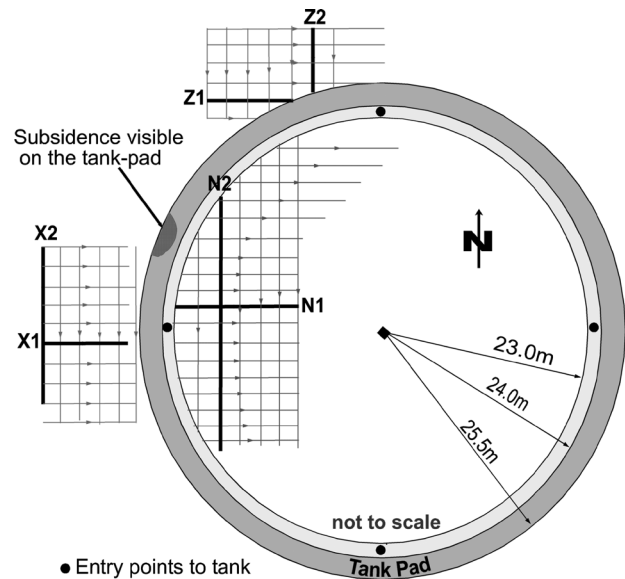


FIGURE 2
Plan of SFGPR survey lines, on and outside the tank-pad.

standing the cause of subsidence and after grouting for evaluating the efficacy of grouting.

DATA PROCESSING AND ANALYSIS

As is well-known, the first step in the processing of GPR data is removal of the dominant effect of direct coupling and other coherent signals between the antenna pair. The further signal processing steps in sequential order are given below.

- Optimizing the frequency range of the maximum response from the subsurface: for this, a Hanning window of 50–200 MHz was selected based on the resonant frequency spectrum analysis over the area. The SFGPR data are in the frequency domain and this enables easy application of the windowing operation.
- Enhancing the small amplitude reflections from the subsurface: for this, an exponential gain function of 20 dB was applied across the first 100 samples.
- Removing the coherent noise (both internal and external): this involves a background subtraction procedure wherein the average of all the signals was subtracted from each of the traces.
- Presence of clutter renders identification of features within subsurface reflections difficult. In such cases, analysis of the magnitude and phase of the complex signal might give an additional clue for target identification or about its attributes (Patterson and Cook 2000; Nuzzo *et al.* 2002). The plot of the magnitude of the complex signal is useful to understand the strength of reflection and the corresponding size and geometry of the subsurface target, while the phase helps to understand change in the physical property of the subsurface medium, thereby enabling demarcation of the target. In case

of SFGPR, the data acquired are in the frequency domain. Hence, it becomes easier to read the magnitude from the complex signal. In this analysis, the magnitude was useful in resolving subsurface reflections of the radar signal. The inverse fast Fourier transform (IFFT) algorithm was then applied over the complex signal to obtain the plot of magnitude (radargram of magnitude). This is equivalent to carrying out complex signal analysis (Taner *et al.* 1979) using the Hilbert transform in the time domain.

Such analysis was done for the data of all the SFGPR profiles (Fig. 2) and subsurface images using raw data and magnitude were generated. The images, obtained before grouting, were examined for presence of subsurface defects and their probable

continuity. Images after grouting were analysed in the same manner to check for remnant defects and evaluate efficacy of grouting. Reflections in time were converted to depth using the velocity (10–10.5 cm/ns) of the GPR waves in the subsurface area.

RESULTS AND DISCUSSION

Images before grouting

A few representative radargrams of the processed SFGPR data (along the highlighted orthogonal lines in Fig. 2) are discussed here. Figure 3 is the plot of SFGPR raw data (inside the tank) along the lines N1 (Fig. 3a) and N2 (Fig. 3b) showing weak to moderately strong reflections. But, when the magnitude was plotted separately, as in Fig. 4 (N1 – Fig.4a and N2 – Fig.4b), an enhanced pattern of reflections was observed. Similarly, the

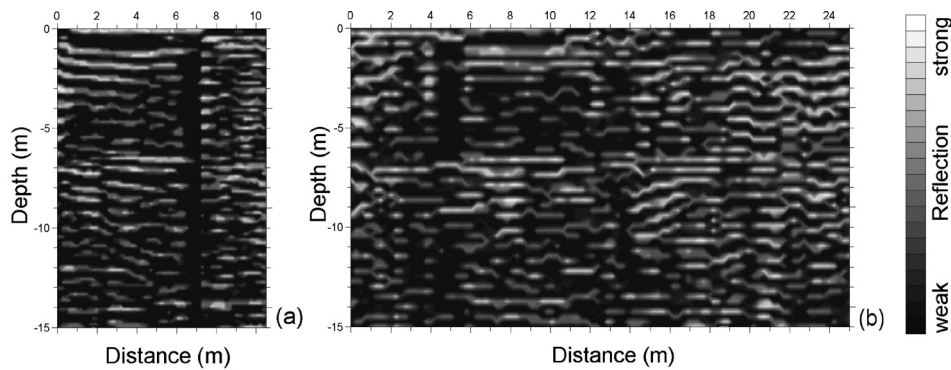


FIGURE 3 Radargrams of raw SFGPR data along lines N1(a) and N2(b) as shown in Fig. 2.

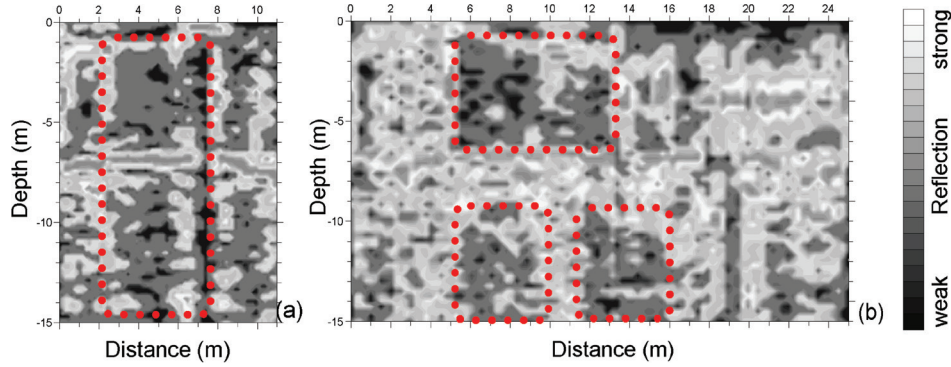


FIGURE 4 Radargrams of magnitude along lines N1(a) and N2(b).

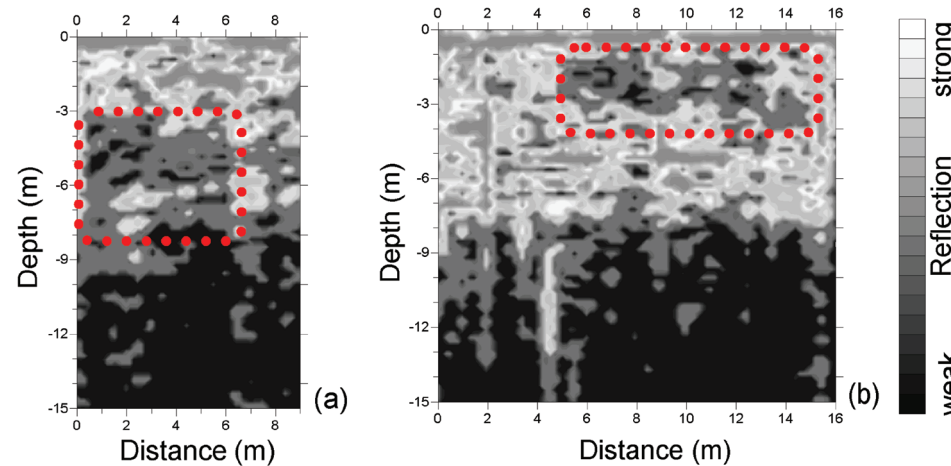


FIGURE 5 Radargrams of magnitude along lines X1(a) and X2(b) as shown in Fig. 2.

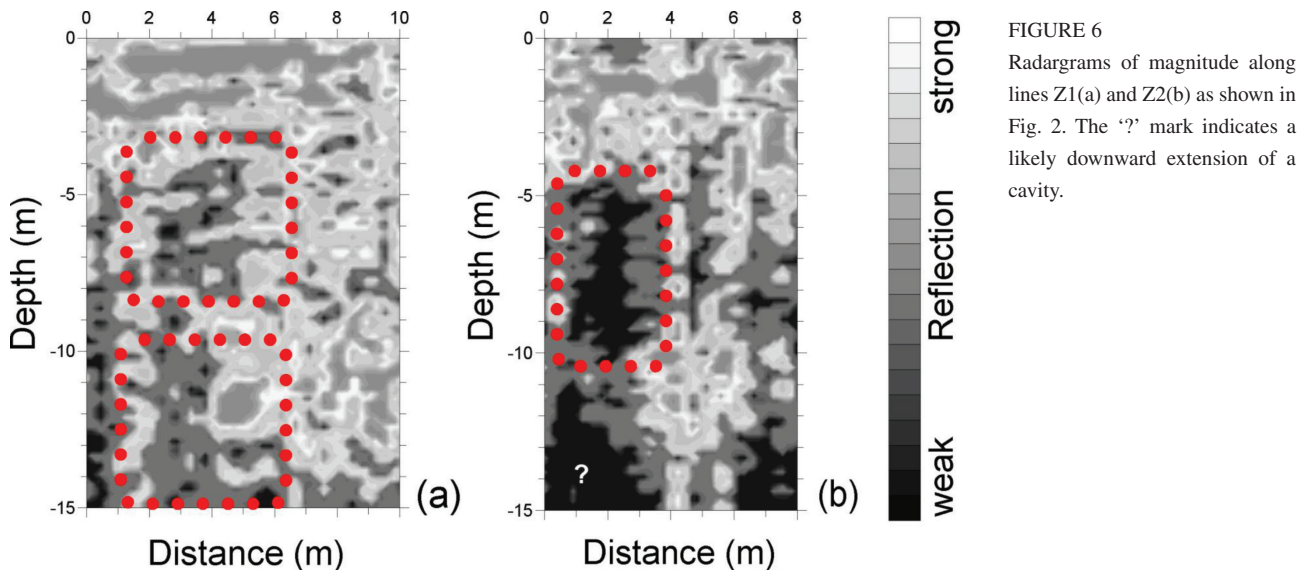


FIGURE 6 Radargrams of magnitude along lines Z1(a) and Z2(b) as shown in Fig. 2. The ‘?’ mark indicates a likely downward extension of a cavity.

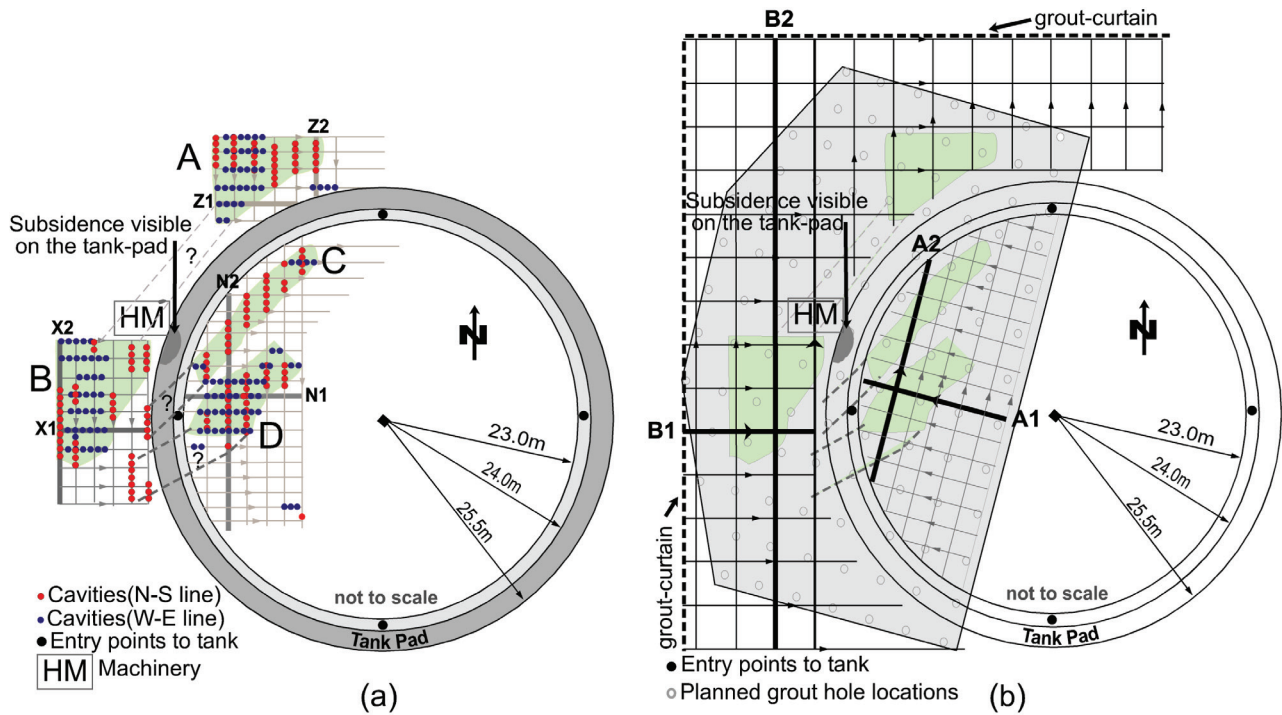


FIGURE 7 (a) Schematic plan view of the groups of cavities (A, B, C and D) detected before grouting. (b) Shaded area showing boreholes designed for grouting; superimposed is the plan of the SFGPR survey lines, after grouting.

magnitude images were generated for lines (X1, X2 and Z1, Z2 in Fig.2) outside the tank periphery, on the western (Fig. 5) and northern (Fig. 6) flanks of the tank. Figure 5 shows the magnitude images of the subsurface corresponding to the two profiles, X1 (Fig. 5a) and X2 (Fig. 5b) and Fig. 6 represents the image corresponding to the northern flank of the tank along the Z1 (Fig. 6a) and Z2 (Fig. 6b) lines. Interestingly, the pattern of reflections in all these radargrams shows subsurface features

resembling the geometry of a cavity (indicated by the dots in Figs 4–6). The pattern of reflections on the radargrams of all the lines strongly indicated the presence of cavities along several of these lines. Small (≤ 2 m) to large (≥ 6 m) size cavities were seen in the radargrams, in the depth range of 2–15 m from the surface. Their extent along the profiling direction ranged between 3–12 m. The extent of the cavities (along the direction of profiling) measured on the radargrams was translated (red and blue

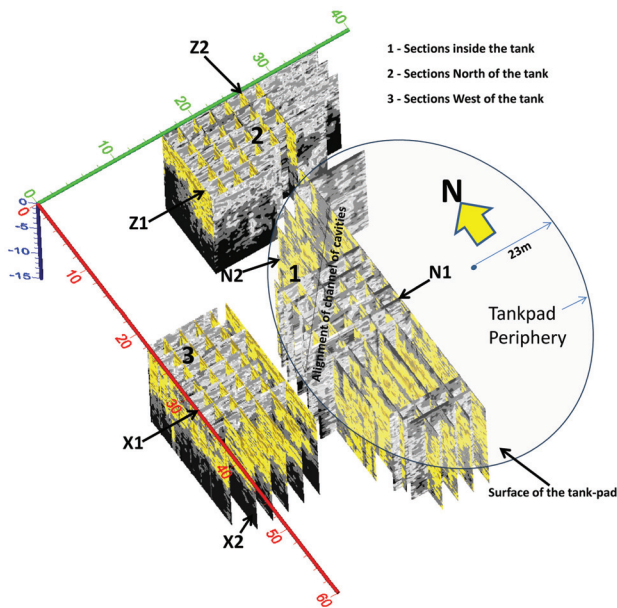


FIGURE 8
3D perspective view of the SFGPR sections taken before grouting. An arrow above the sections inside the tank indicates the likely alignment of cavities. Periphery of the tank-pad is superimposed to aid visualization.

dots, Fig. 7a) on to the plan of the survey lines. Four groups of cavities (A, B, C and D) were identified concentrating in the subsurface. A and B were located outside the tank-pad (north and west), while C and D were located in the north-western area of the tank-pad, inside the tank. Combined visualization of such a translation indicated a probable connectivity (indicated by the dotted lines and “?” mark) between the cavities imaged over successive lines, pointing to a possibility of existence of channel-like features trending in the direction of north to west.

The existence of a series of such localized cavities was not expected in compact and hard lateritic soil. Dissolution of soft minerals by subsurface water flow or leaching phenomena in the lateritic soils could have been one of the causes of the formation of such cavities, which were probably partially filled or were not filled within compact and hard lateritic soil. Also, previous history of the place revealed existence of a few small villages and adjoining agricultural lands before construction of the refinery. Open water-wells were part of the agricultural lands. There was a possibility of such water-wells not fully filled and consolidated during excavation and levelling operations. Such poorly filled water-wells, resembling a large partially filled cavity, could have been a potential area of weakness in the subsurface surrounded by compact and hard soil.

Such cavities in the subsurface have rendered the ground incompetent and could have been the primary cause of subsidence in the north-western area. The cavities (north-west) could have coalesced in an inelastic compaction under the load of a filled storage tank, leading to localized subsidence of the ground and the tank-pad, and the subsequent damage to the oil tank.

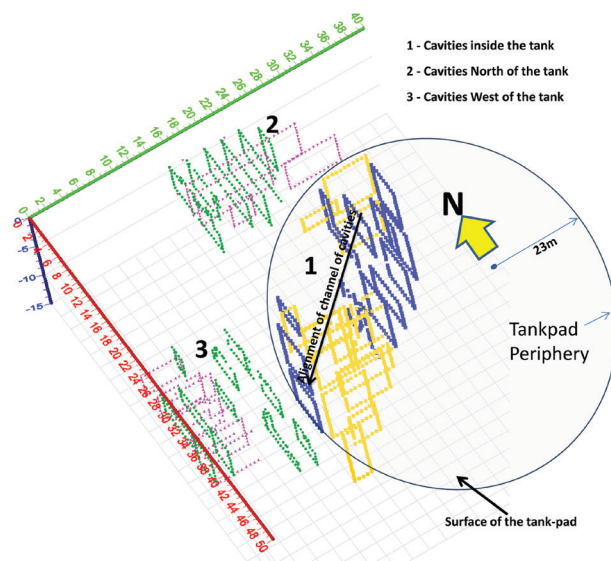


FIGURE 9
3D perspective view of the outline of the cavities before grouting. N-S trending cavities are shown in green and blue; W-E trending cavities are shown in pink and yellow. Periphery of the tank-pad is superimposed to aid visualization.

The entire data set was acquired in a dense grid pattern and this enabled the generation of a 3D image. A 3D view (Grasmueck 2002) of SFGPR data is useful in overcoming the limitations in presenting the spatial distribution of subsurface cavities. To facilitate visualization of the cavity distribution in the subsurface, the intersecting 2D magnitude plots are presented in a 3D perspective view in Fig. 8, with the 2D section of each line presented in a respective co-ordinate plane. The 3D visualization reveals the trend or alignment (indicated by an arrow) of the cluster of the subsurface cavities. An extract of the cluster of cavities (Fig. 9) is presented separately, again in perspective view, in order to improve clarity in the viewing of subsurface cavities. The foundation area below the tank-pad was infested with cavities amounting to 690 m³ while the subsurface surrounding the tank had 720 m³ of cavity volume. Thus, out of the 9300 m³ of the subsurface scanned, 1410 m³ was found occupied by the cavities, most of which were clustered around the visible subsidence in the tank-pad. These cavities had to be plugged in order to make the subsurface competent enough to bear the load of the oil-filled tank.

Grouting in the foundation

Once the existence of cavities trending in a channel-like feature was established, the affected subsurface area was reinforced by grouting so as to prevent the collapse of cavities and subsequent subsidence of ground below the tank-pad. This reinforcement was carried out by three-stage grouting in depth ranges of 0–6 m, 6–12 m and 12–18 m at various grout pressures. The borehole array for grouting was designed in a grid-array at 5 m grid nodes

to cover the entire affected area (shaded polygon, Fig. 7b), based on the results of the SFGPR survey. Besides, curtain grouting (Fig. 7b) was done on the northern and western boundaries to isolate the subsurface of the tank-pad from possible connectivity with any such cavities in the vicinity of the tank-pad.

Images after grouting

In order to check the efficacy of grouting in the foundation, a SFGPR survey along various lines was carried out once again both inside and outside the tank (northern and western flanks). This time the survey area was expanded to cover the entire grouted area (Fig. 7b) and imaging was done up to 20 m depth to cover the deepest level of grouting. SFGPR data collected after the grouting were processed in the same manner as done for the pre-grouting stage. Figures 10 and 11 represent the subsurface images after grouting along the SFGPR profiles inside (A1 and A2) and outside (B1 and B2) the tank respectively. In order to confirm the efficacy of grouting, the raw images were also plotted and comparative analysis was done with the corresponding magnitude plots. In both the forms of images (magnitude and raw), absence of previously seen reflections indicated that the cavities detected earlier in the subsurface were grouted. Radargrams along a few lines showed the cavities either remained ungrouted or only partially grouted. Significant changes in the plots of magnitude of

reflections were observed wherein the pattern of reflections observed before grouting, in and around the cavities, was conspicuously absent. The reflections are normalized plots based on peak magnitudes and hence, the presence of any remnant cavities was confirmed by a combination of a pattern and strength of reflection magnitudes around the same location.

The 2D sections generated during this phase were again projected in a 3D form as in Fig. 12. While the absence of signatures resembling cavities is quite conspicuous, there were some remnant cavities or poorly grouted pockets in the subsurface that are not quickly visible. Hence, to enable viewing of the remnant cavities, a 3D view of their distribution is presented in Fig. 13. The volume of such remnant cavities or weak-zones amounted to 215 m³, which is 15% of the previously detected volume of the cavities. Such poorly grouted locations were recommended for grouting again. Thus, except a few locations in the subsurface, due to not fully grouted cavities, the SFGPR images confirmed the grouting was effective. Considering the necessity of a uniformity of load bearing strength of the foundation regime, all such suspected remnant cavities were grouted again. Later, the tank-pad was tested with standard procedures. When no failure or any other anomalous behaviour was observed even after repeated tests, this tank was inducted into production line-up as initially designed.

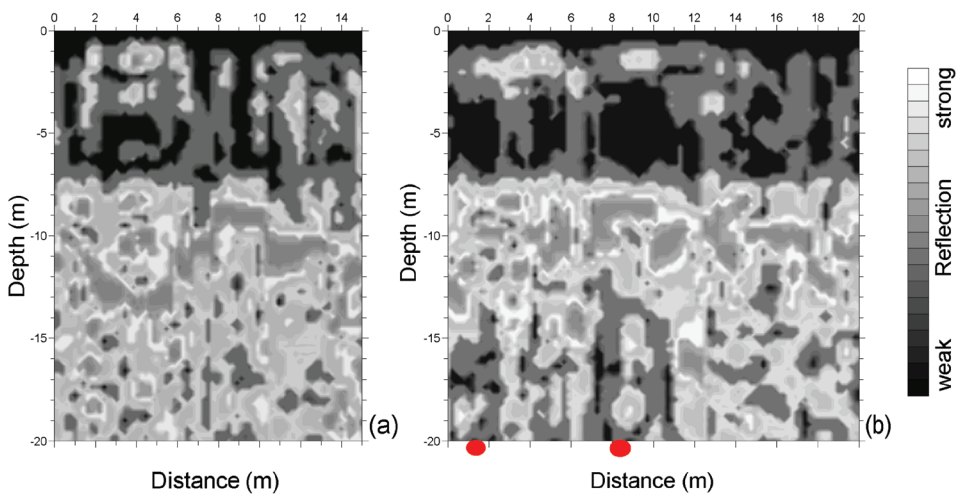


FIGURE 10 Radargrams of magnitude along lines A1(a) and A2(b) inside the tank, as shown in Fig. 7(b), wherein the pattern of reflections interpreted as cavities is absent after grouting. The two red dots indicate poorly grouted locations at the bottom of the section.

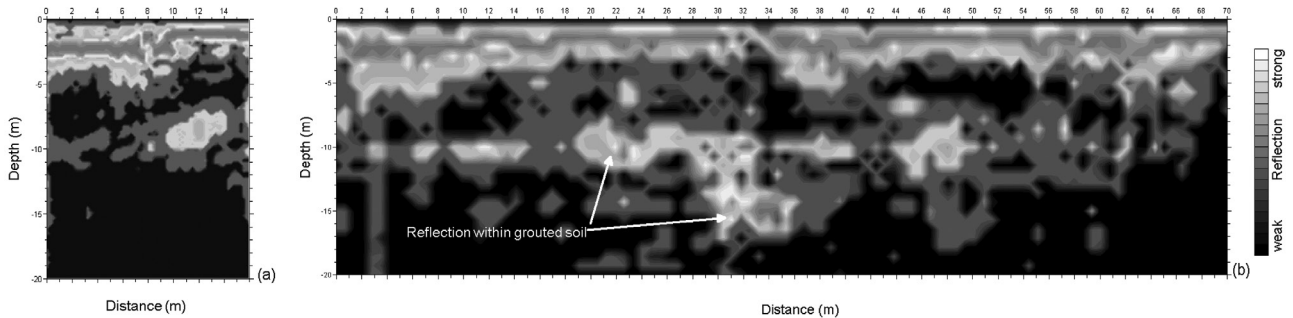


FIGURE 11 Radargrams of magnitude along lines B1(a) and B2(b) outside the tank, as shown in Fig. 7(b), with no signature of cavities.

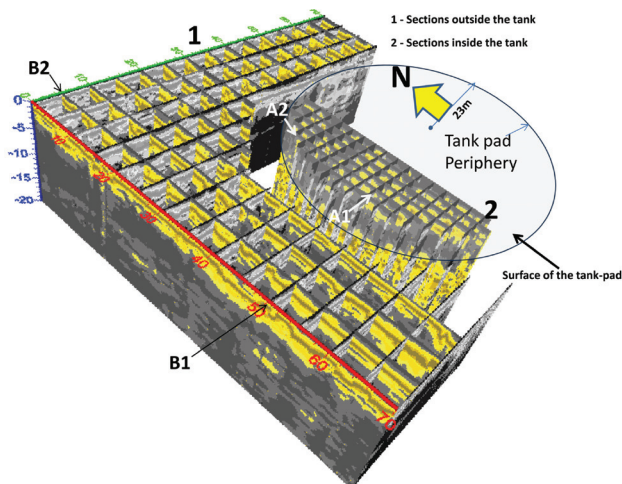


FIGURE 12
3D perspective view of the SFGPR sections, after grouting, indicating absence of cavities. Periphery of the tank-pad is superimposed to aid visualization.

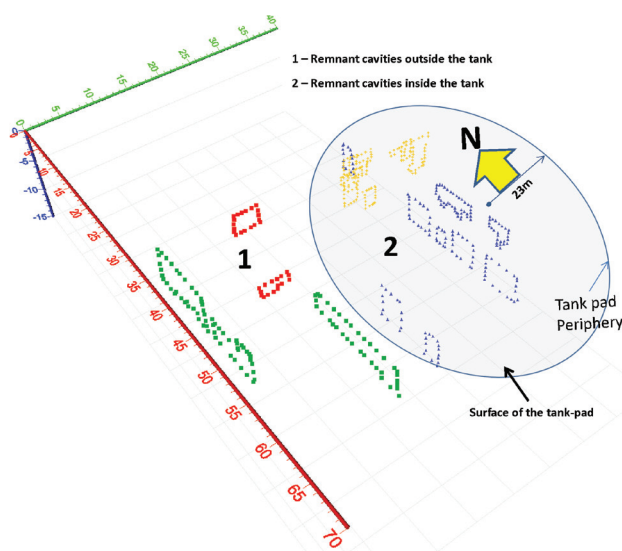


FIGURE 13
3D perspective view of the outline of the remnant cavities, after grouting. Periphery of the tank-pad is superimposed to aid visualization.

CONCLUSIONS

In this paper, the successful application of SFGPR in imaging the subsurface cavities, before and after grouting, in the foundation of the tank was discussed. The advantage of the frequency domain GPR in choosing the site specific frequency spectrum and the ease of making use of the magnitude of the complex signal (analogous to the Hilbert transformed time domain signal) helped significantly in distinguishing the subsurface cavities in an otherwise non-coherent clutter background. The reinforcement of the foundation involved systematic drilling of grouting holes, which were designed based on the pre-grouting results of

the SFGPR survey. A comparative analysis of the subsurface images (2D and 3D), before and after the grouting operation, aided the quantification of volume occupied by the subsurface cavities and the extent to which the subsurface of the tank was grouted.

In this study, SFGPR was fairly effective and economically useful in facilitating complete restoration of the foundation of the oil tank. More than its use for diagnostic investigations, timely application of such a non-destructive tool will be useful to prevent unexpected damage and mitigate potential hazards at engineering construction sites.

ACKNOWLEDGMENTS

The authors are thankful to the oil refinery company for their support in accomplishing the work. The authors are also thankful to the Director, NIRM for permission to publish this work. Timely preparation of inputs, for 2D/3D figures, by our colleagues Mr. Butchi Babu and Mr. Y.V. Sivaram is sincerely acknowledged. Support of colleagues was useful in accomplishing and presenting the SFGPR imaging work.

REFERENCES

- Ballard R.F., Cuenod Y. and Jenni J.P. 1983. Detection of karst cavities by geophysical methods. *Bulletin of International Association of Engineering Geology* **26–27**, Paris.
- Bavusi M., Giocoli A., Rizzo E. and Lapenna V. 2009. Geophysical characterisation of Carlo's V Castle (Crotona, Italy). *Journal of Applied Geophysics* **67**(4), 386–401. doi:10.1016/j.japgeo.2008.09.002
- Benson A.K. 1995. Applications of ground penetrating radar in assessing some geological hazards: Examples of groundwater contamination, faults, cavities. *Journal of Applied Geophysics* **33**(1–3), 177–193. doi:10.1016/0926-9851(95)90040-3.
- Beres M., Luetscher M. and Olivier R. 2001. Integration of ground penetrating radar and microgravimetric methods to map shallow caves. *Journal of Applied Geophysics* **46**(4), 249–262. doi:10.1016/S0926-9851(01)00042-8
- Branston M.W. and Styles P. 2006. Site characterization and assessment using the microgravity technique: A case history. *Near Surface Geophysics* **4**(6), 377–385. doi: 10.3997/1873-0604.2006011
- Butler D.K. 1984. Microgravimetric and gravity gradient techniques in detection of subsurface cavities. *Geophysics* **49**(7), 1084–1096. doi:10.1190/1.1441723
- By T.L., Kong F.N. and Westerdahl H. 1992. Georadar development at the Norwegian Geotechnical Institute (NGI). *Proceedings of the 4th International Conference on GPR (GPR'92)*, Rovaniemi, Finland, 21–28.
- Cardarelli E., Di Filippo G. and Tuccinardi E. 2006. Electrical resistivity tomography to detect buried cavities in Rome: A case study. *Near Surface Geophysics* **4**(6), 387–392. doi: 10.3997/1873-0604.2006012
- Chamberlain A.T., Sellers W., Proctor C. and Coard R. 2000. Cave Detection in Limestone using Ground Penetrating Radar. *Journal of Archaeological Science* **27**(10), 957–964. doi:10.1006/jasc.1999.0525
- Cook J.C. 1965. Seismic mapping of underground cavities using reflection amplitudes. *Geophysics* **30**(4), 527–538. doi:10.1190/1.1439618
- Daniels J.J. 1988. Locating caves, tunnels and mines, *Geophysics. The Leading Edge* **7**(3), 32–52. doi:10.1190/1.1439492
- Daniels D.J. 1996. *Surface Penetrating Radar, IEE Radar, Sonar, Navigation and Avionics Series 6*. The Institution of Electrical Engineers (IEE), London.

- Davis J.L. and Annan A.P. 1989. GPR for high resolution mapping of soil and rock stratigraphy. *Geophysical Prospecting* **37**(5), 531–551. doi:10.1111/j.1365-2478.1989.tb02221.x
- Grasmueck M. 2002. 3D GPR reveals complex internal structure of Pleistocene oolitic sandbar. *The Leading Edge* **21**(7), 634–639. doi:10.1190/1.1497315
- Hamran S.E., Gjessing D.T., Hjelmstad J. and Aarholt E. 1995. Ground penetrating synthetic pulse radar: Dynamic range and modes of operation. *Journal of Applied Geophysics* **33**(1–3), 7–14. doi:10.1016/0926-9851(95)90025-X
- Jha P.C., Balasubramaniam V.R., Nelli S., Sivaram Y.V. and Gupta R.N. 2006. Application of GPR survey for foundation evaluation studies – A case study with oil storage tank. *Proceedings of the 11th International Conference of Ground Penetrating Radar (GPR 2006)*, Columbus, Ohio, USA.
- Jha P.C., Balasubramaniam V.R. and Sivaram Y.V. 1999. Site characterisation for location of oil storage tanks: A case study. *Proceedings of the International Conference on Rock Mechanics and Site Characterisation (ROCKSITE-99)*, December 6–8, 1999, Bangalore, India, 255–262.
- Kong F.N. and By T.L. 1995. Performance of a GPR system which uses Step Frequency Signals. *Journal of Applied Geophysics* **33**(1–3), 15–26. doi.org/10.1016/0926-9851(95)90026-8
- Labuda T.Z. and Baxter A.C. 2001. Mapping karst conditions using 2D and 3D resistivity imaging methods. *Proceedings of the Symposium on the Application of Geophysics to Engineering and Environmental Problems (SAGEEP) 14*, Environmental and Engineering Geophysical Society, Denver, Colorado, USA. doi:10.4133/1.2922906
- Langman A. and Ingg M.R. 2001. Pulse versus stepped frequency continuous wave modulation for ground penetrating radar. *Proceedings of International Geoscience and Remote Sensing Symposium, (IGARSS'01)*, IEEE, 1533–1535. doi:10.1109/IGARSS.2001.976902
- Leckebusch J. 2011. Comparison of a stepped-frequency continuous wave and a pulsed GPR System. *Archaeological Prospection* **18**, 15–25. doi:10.1002/arp.396
- Lizuka K., Freundorfer A.P., Wu K.H., Moil H., Ogura H. and Nguyen V.K. 1984. Step-frequency radar. *Journal of Applied Physics* **56**(9), 2572–2583. doi:10.1063/1.334286
- Miller R.D. and Steeples D.W. 1991. Detecting voids in a 0.6m coal seam, 7m deep using seismic reflection. *Geoexploration* **28**, 109–119. doi:10.1016/0016-7142(91)90043-C
- Mochales T., Casas A.M., Pueyo E.L., Pueyo O., Román M.T., Poció A. et al. 2008. Detection of underground cavities by combining gravity, magnetic and ground penetrating radar surveys: A case study from the Zaragoza area, NE Spain. *Environmental Geology* **53**, 1067–1077. doi:10.1007/s00254-007-0733-7
- Noon D.A., Longstaff I.D. and Yelf R.J. 1994. Advances in the development of SFGPR. *Proceedings of the 5th International Conference on Ground Penetrating Radar (GPR'94)*, Kitchener, Ontario, Canada, 117–132, June 12–16, 1994.
- Nuzzo L., Leucci G., Negri S., Carozzo M.T. and Quarta T. 2002. Application of 3D visualization techniques in the analysis of GPR data for archaeology. *Annals of Geophysics* **45**(2), 321–337.
- Olhoft G.R. 1998. Electrical, magnetic, and geometric properties that determine ground penetrating radar performance. *Proceedings of the 7th International Conference (GPR98)*, Lawrence, KS, USA, 177–182.
- Patterson J.E. and Cook F.A. 2000. The application of complex trace analysis for improved target identification in gem tourmaline bearing pegmatites. *Proceedings of the 8th International Conference on GPR (GPR2000)*, 653–657.
- Pellerin L. 2002. Applications of electrical and electromagnetic methods for environmental and geotechnical investigations. *Surveys in Geophysics* **23**, 101–132.
- Robinson L.A., Weir W.B. and Young L. 1974. Location and Recognition of Discontinuities in Dielectric Media Using Synthetic RF Pulses. *IEEE Proceedings* **62**(1), 36–44. doi:10.1109/PROC.1974.9383
- Rybakov M., Rotstein Y., Shirman B. and Al-Zoubi A. 2005. Cave detection near the Dead Sea – A micromagnetic feasibility study. *The Leading Edge, Society of Exploration Geophysicists* **24**(6), 585–590. doi:10.1190/1.1946210
- Stickley G.F., Noon D.A., Cherniakov M. and Longstaff I.D. 2000. Gated stepped-frequency ground penetrating radar. *Journal of Applied Geophysics* **43**(2–4), 259–269. doi:10.1016/S0926-9851(99)00063-4
- Taner M.T., Koehler F. and Sheriff R.E. 1979. Complex seismic trace analysis. *Geophysics* **44**, 1041–1063. doi:10.1190/1.1440994
- Xu X., Zeng Q., Li D., Wu J., Wu X. and Shen J. 2010. GPR detection of several common subsurface voids inside dikes and dams. *Engineering Geology* **111**, 31–42. doi:10.1016/j.enggeo.2009.12.001